

Supramolecular Toxin Complexes for Targeted Pharmacological Modulation of Polymorphonuclear Leukocyte Functions

Astrid Johanna Heck, Theresa Ostertag, Leonie Schnell, Stephan Fischer, Bikram Keshari Agrawalla, Pia Winterwerber, Eva Wirsching, Michael Fauler, Manfred Frick, Seah Ling Kuan,* Tanja Weil,* and Holger Barth*

The targeted pharmacological modulation of polymorphonuclear leukocytes (PMNs) is of major medical interest. These innate immune cells play a central role in the defense against pathogenic microorganisms. However, their excessive chemotactic recruitment into tissues after traumatic injury is detrimental due to local and systemic inflammation. Rho-GTPases, being the master regulators of the actin cytoskeleton, regulate migration and chemotaxis of PMNs, are attractive pharmacological targets. Herein, supramolecular protein complexes are assembled in a “mix-and-match” approach containing the specific Rho-inhibiting clostridial C3 enzyme and three PMN-binding peptides using an avidin platform. Selective delivery of the C3 Rho-inhibitor with these complexes into the cytosol of human neutrophil-like NB-4 cells and primary human PMNs *ex vivo* is demonstrated, where they catalyze the adenosine diphosphate (ADP) ribosylation of Rho and induce a characteristic change in cell morphology. Notably, the complexes do not deliver C3 enzyme into human lung epithelial cells, A549 lung cancer cells, and immortalized human alveolar epithelial cells (hAELVi), demonstrating their cell type-selectivity. The supramolecular complexes represent attractive molecular tools to decipher the role of PMNs in infection and inflammation or for the development of novel therapeutic approaches for diseases that are associated with hyperactivity and reactivity of PMNs such as post-traumatic injury.

body, molecules derived from microbial pathogens and/or the host, recruit PMNs via chemotactic mechanisms from the blood stream to sites of infection. PMNs evade from the blood vessels into the tissue to ingest the pathogenic microorganisms by phagocytosis and to eliminate bacteria and fungi via their arsenal of cytotoxic substances. However, besides the beneficial role of PMN activity with infections, hyperactivity of PMNs can be detrimental for patients, if PMNs are excessively recruited into injured tissues.^[1] Such conditions are, for example, reported for multiple injured patients suffering from blunt thorax trauma, where the enhanced chemotactic recruitment of PMNs and monocytic cells into the lungs and the subsequent release of their toxic mediators enhance the alveolar barrier breakdown resulting in local and systemic inflammation and contributing to the poor outcome of such patients.^[1–6]


Therefore, the targeted, cell type-selective, pharmacological inhibition of excessive chemotactic recruitment of PMNs

1. Introduction

Polymorphonuclear leukocytes, also termed PMNs or neutrophils, are the most abundant leukocytes in human blood and a major component of the innate immune system. In the human

will enhance our understanding of their role in the first-line defense against microbes and their contribution to the excessive inflammatory responses after traumatic tissue injury. Since migration, chemotaxis, and phagocytosis of PMNs depend on the remodeling of the actin cytoskeleton, which is regulated by

A. J. Heck, Dr. B. K. Agrawalla, P. Winterwerber, Dr. S. L. Kuan, Prof. T. Weil
Max Planck Institute for Polymer Research
Ackermannweg 10, 55128 Mainz, Germany
E-mail: kuan@mpip-mainz.mpg.de; weil@mpip-mainz.mpg.de

 The ORCID identification number(s) for the author(s) of this article can be found under <https://doi.org/10.1002/adhm.201900665>.

© 2019 The Authors. Published by WILEY-VCH Verlag GmbH & Co. KGaA, Weinheim. This is an open access article under the terms of the Creative Commons Attribution License, which permits use, distribution and reproduction in any medium, provided the original work is properly cited.

The copyright line for this article was changed on 16 August 2019 after original online publication.

T. Ostertag, Dr. L. Schnell, Dr. S. Fischer, Prof. H. Barth
Institute of Pharmacology and Toxicology – Ulm University Medical Center
Albert-Einstein-Allee 11, 89081 Ulm, Germany
E-mail: holger.barth@uni-ulm.de

E. Wirsching, M. Fauler, Prof. M. Frick
Institute of General Physiology – Ulm University
Albert-Einstein-Allee 11, 89081 Ulm, Germany

Dr. S. L. Kuan, Prof. T. Weil
Institute of Inorganic Chemistry I
Ulm University
Albert-Einstein-Allee 11, 89081 Ulm, Germany

DOI: 10.1002/adhm.201900665

Rho-GTPases,^[7–12] PMN-selective Rho inhibition represents an attractive strategy to downmodulate excessive PMN recruitment from blood into tissues after traumatic injury.^[13] Moreover, PMN-selective molecules modulating Rho-signaling and actin dynamics of these immune cells certainly offer great potential as molecular tools in cell biology and experimental pharmacology to decipher the role of PMN activity in both infection and inflammation. In this context, the C3 enzymes from *Clostridium* (*C.*) *botulinum* (C3bot1) and *C. limosum* (C3lim) are of major interest as they represent the only known specific Rho inhibitors.^[6,10,14–16] C3 proteins are taken up into the cytosol of monocytic cells where they catalyze the specific mono-ribosylation of Rho A and Rho B. This inhibits Rho-signaling resulting in the reorganization of actin filaments accompanied by a characteristic change in cell morphology.^[11,17–21] Recently, it has been demonstrated by our groups that the targeted pharmacological inhibition of Rho activity by C3 enzyme inhibits the migration and chemotaxis of primary human monocytes *ex vivo*.^[11] Moreover, the local intra-tracheal application of this Rho-inhibitor prevented the excessive recruitment of monocytic cells from the blood into the lungs of mice after blunt thorax trauma.^[11] However, the C3 Rho-inhibitor has no effect on PMNs *ex vivo* and does not reduce the amount of PMNs in the lungs of mice after blunt thorax trauma.^[11] Therefore, the selective introduction of C3 Rho-inhibitor into PMNs would be highly desirable for such applications.

Herein, we developed PMN-selective Rho-inhibitors based on the supramolecular assembly of C3 Rho-inhibitor and specific PMN-targeting peptides on an avidin (Avi) platform to provide cell-type selectivity. The PMN-targeting peptide sequences have previously been identified using random peptide phage display that addresses the neutrophils specifically.^[22–24] For instance, the Ac-GGPNLTGRWGPPVESALAK-NH₂ (GGP) sequence reveals neutrophil and monocyte selective binding, which has been applied to liposomes for targeted delivery.^[25] In addition, the peptide cinnamoyl-F(D)LF(D)LFK-NH₂ (FK), an antagonist of the formyl peptide receptor 1 (FPR-1) of neutrophils, has been conjugated to imaging agents or nanoparticles for *in vivo* imaging.^[26,27]

Although peptide sequences such as GGP could be recombinantly fused to C3 Rho-inhibitor, the expression of C3 enzyme with cyclic or chemically modified peptides, such as FK cannot be achieved by molecular biology techniques. Furthermore, the fusion of multiple peptide sequences to a single enzyme is challenging by genetic means and would require tedious optimization.^[28,29] Release characteristics are controlled by chemical linker design to impart a variety of stimulus-responsive groups for, e.g., pH-controlled release in acidic endosomal vesicles or inside the cytoplasm of cancer cells, which is also challenging to achieve by genetic engineering.^[30] Hence, there is a great interest in novel “chemistry” methods to design and produce customized protein drugs.^[31,32] In particular, supramolecular assembly of protein complexes provides convenient access to sophisticated multiprotein architectures that cannot be achieved by molecular biology methods.^[31]

The assembly of multiprotein complexes that contained functional subunits of bacterial protein toxins and dendrimers^[33,34] or multiple copies of the cancer-cell targeting peptide somatostatin at an avidin platform has been established by our groups before. Recently, we have reported the

selective delivery of a supramolecular complex that contains the Rho-inhibitor C3bot1 (henceforth C3) and somatostatin as cell-targeting peptide into the cytosol of human cancer cells overexpressing the somatostatin receptor, resulting in reduced growth of a human xenograft lung tumor.^[35] The best effect was achieved when three somatostatin peptides and one C3 enzyme were bound to the avidin platform presumably via the multivalency effect.^[35] We further expand on this versatile strategy and report herein for the first time the stoichiometric-controlled assembly of 1) multiple copies of different PMN-targeting peptides and 2) C3 Rho-inhibitor via 3) a pH-cleavable hydrazone linker for controlled intracellular release of the C3 enzyme into the cytosol of PMNs (Figure 1). Our platform allows rapid generation of different supramolecular toxin combinations, e.g., by varying the PMN-targeting peptides, which is highly desirable for throughput synthesis and screening to evaluate the efficacy of the different combinations of the C3 Rho-inhibitor and different PMN targeting peptide sequences. We believe that our approach offers great potential for the development of cell type-selective biotherapeutics for the targeted treatment of local and systemic inflammation, e.g., after traumatic injury of multiple injured patients in a convenient “mix-and-match” assembly.

2. Results and Discussion

2.1. “Mix-and-Match” Assembly and Characterization of the Supramolecular Complexes (GGP)₃-Avi-C3 and (FK)₃-Avi-C3

The supramolecular complexes (GGP)₃-Avi-C3 and (FK)₃-Avi-C3 containing the PMN-targeting peptides GGP and FK as well as C3 (Figure 1) were both designed based on avidin–biotin technology. Avidin (Avi), the central platform for assembly, is a tetrameric protein (pI > 9) that forms strong noncovalent interactions ($K_d = 10^{-15}$ M) with its natural binding partner biotin at four binding sites. Here, Avi is selected as a monodisperse supramolecular “glue” to combine the PMN-targeting peptides and C3 Rho-inhibitor at spatially distinct locations. To incorporate biotin into the Ac-GGPNLTGRWGPPVESALAK-NH₂ (GGP) sequence, GGP was functionalized using a bifunctional maleimide-biotin with a short ethylene glycol linker (compound 1, Figure 2A) that improves water solubility. The biotinylated GGP (B-GGP) peptide was obtained in 40% yield after high-performance liquid chromatography (HPLC) purification with >95% purity (Figure S4, Supporting Information). The PMN-targeting peptide cinnamoyl-F(D)LF(D)LFK-NH₂ (FK) with a biotin at the C-terminus (Figure 2B) was purchased commercially (PhtdPeptides Co., Ltd. with 95% purity). To control the stoichiometry of peptides with terminal biotin bound to Avi, a competitive binding assay with 2-(4-hydroxyphenylazo)benzoic acid (HABA) was performed. HABA binds to Avi with lower affinity compared to biotin and shows absorbance at 500 nm in the complexed form (Figure 2C). Thus, disappearance of the absorption peak indicates displacement of HABA by biotin. A stepwise reduction in absorbance was observed upon addition of 1–4 equivalents of biotin indicating the controlled binding of the respective biotinylated neutrophil targeting peptide to Avi (Figure 2C).

It was determined that 1.25 mole equiv of B-GGP and 1.0 mole equiv of B-FK are required per binding pocket in Avi,

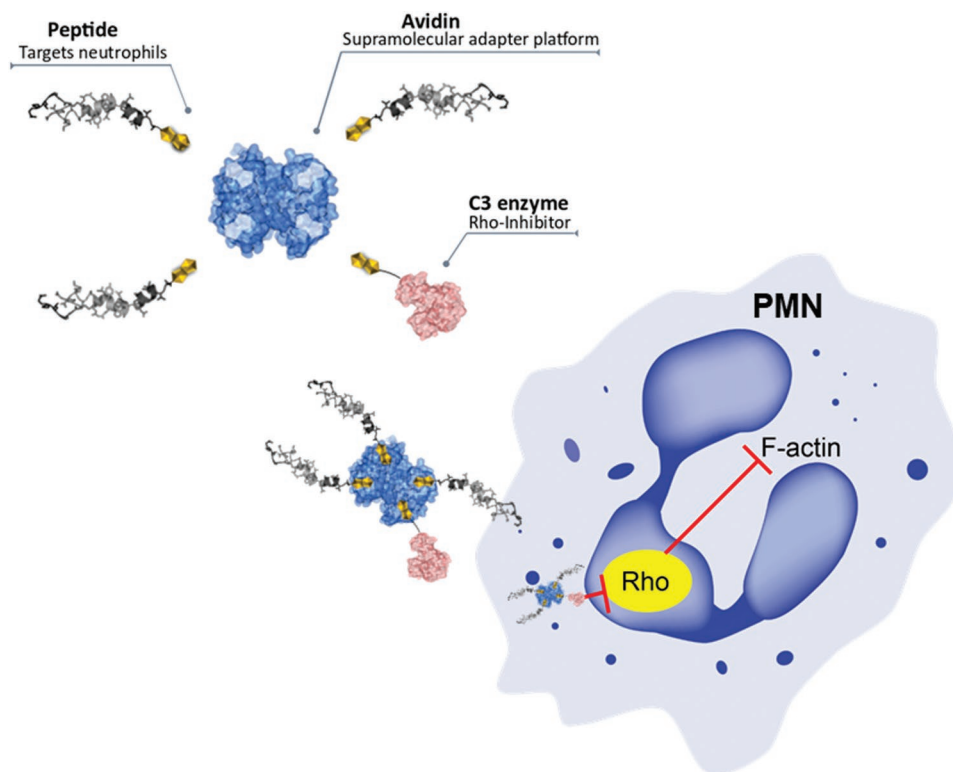


Figure 1. Design and potential mode of action of supramolecular complexes containing specific PMN-targeting peptides and C3-Rho-inhibitor assembled on a central avidin (Avi) platform. The resultant protein complex is designed to selectively internalize into PMNs where the C3-catalyzed Rho-inhibition down-modulates Rho-signaling in order to modulate PMN functions such as migration and chemotaxis.

respectively, most likely for steric reasons. Subsequently, the transporters with three biotinylated peptides per Avi were prepared by mixing the corresponding mole equiv of B-GGP or B-FK with Avi (Figure 2D). These (GGP)₃-Avi or (FK)₃-Avi conjugates offer a free available binding site for conjugation to mono-biotinylated C3.

Next, mono-biotinylation of a cysteine mutant of C3 was accomplished. The enzyme activity and substrate specificity as well as the biological activity of this recombinant C3 variant has been confirmed earlier in J774A.1 macrophages and osteoclast-like RAW 264.7 cells.^[21] A biotin-maleimide conjugation with a pH-sensitive hydrazone linkage (**4**) that allows cleavage at acidic pH was synthesized with modification from a procedure published previously (Figure 3A and Scheme S1, Supporting Information).^[35] The pH-sensitive hydrazone triggers controlled toxin release in acidic endosomal compartments of the cells.^[35] Compound **4** was conjugated to C3 to afford mono-biotinylated C3 (B-C3, Figure 3B) in 78% yield, determined by bicinchoninic acid (BCA) assay and Quant*Tag biotin quantification assay (Figure S3, Supporting Information). The successful biotinylation was determined using Western blot analysis (Figure 5), and the degree of biotinylation was quantified to be 91% using the Quant*Tag Biotin Kit (Figure S3, Supporting Information).

The controlled assembly of (GGP)₃-Avi-C3 and (FK)₃-Avi-C3 was accomplished through stoichiometric control according to the optimized ratio of 1.25 equiv of B-GGP and 1.0 equiv of B-FK per binding pocket (GGP-B:Avi:B-C3 = 3.75:1:1); (B-FK:Avi:B-C3 = 3:1:1, Figure 4A). Sodium dodecyl sulfate polyacrylamide gel electrophoresis (SDS-PAGE) analysis of

(GGP)₃-Avi-C3 and (FK)₃-Avi-C3 with and without heating against a known concentration of B-C3bot1 (Figure 4B) further revealed that nearly all of the C3 protein reacted during the conjugation reaction, confirming the formation of the supramolecular complexes. The height profile of the constructs (3–6 nm) was determined by using atomic force microscopy (AFM) and no larger aggregates were detected indicating sample homogeneity (Figure 4C). Furthermore, no aggregates were detected by dynamic light scattering in solution (Table S1, Supporting Information). The zeta-potential of (FK)₃-Avi-C3 and (GGP)₃-Avi-C3 was determined to be –4.56 and –2.39 mV, respectively, which is consistent with the theoretical isoelectric point (pI) of FK (pI = 6) and GGP (pI = 9) peptides (Table S2, Supporting Information).

Next, the stoichiometry of the complexes was assessed using absorption spectroscopy of dye-labeled constructs. First, (GGP)₃-Avi-C3 was triply labeled with dyes in a controlled fashion: First, Avi was labeled with Alexa-594 dye, B-C3 was functionalized with Alexa-647 dye and GGP with Alexa-488 (details are given in the Supporting Information). The ratio of GGP:Avi:C3 was determined from the absorption envelopes using a multiplate reader and a ratio of 3.2:1:0.7 was calculated (Figure 4B). Similarly, absorbance measurement of a dual-labeled (FK)₃-Avi-C3 construct was determined to give a ratio of Avi:C3 of 1:0.8 (Figure S7, Supplementary Information).

The assembly and pH-induced release was further demonstrated with the construct, (FK)₃-Avi-C3, through fluorescence resonance energy transfer (FRET) study (Figure 5A). The labeled proteins and peptides were prepared as outlined in

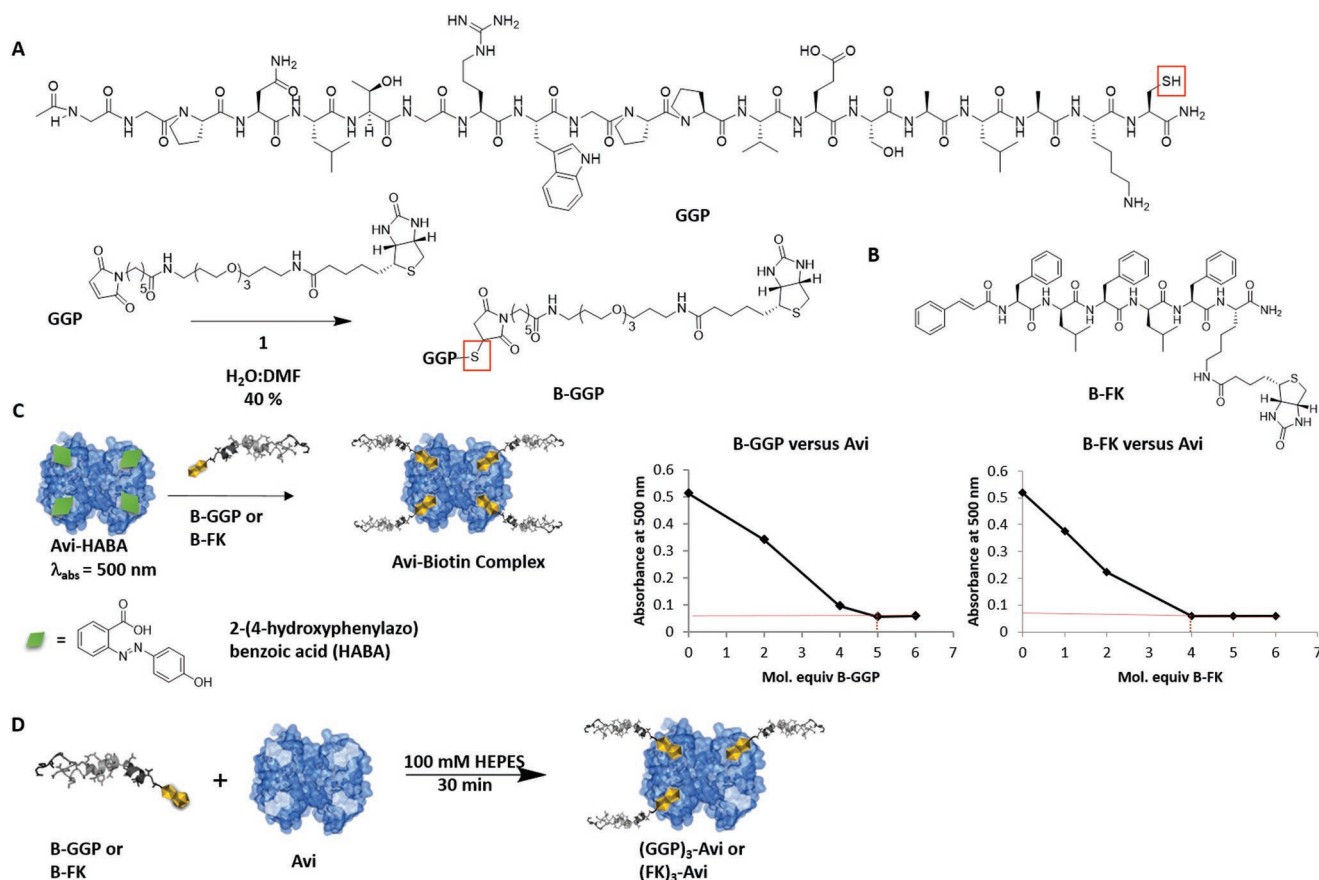


Figure 2. A) Synthesis of biotinylated GGP (B-GGP, H₂O:DMF, 1:0.5, 7.5 mL), room temperature, overnight, 40% isolated yield. B) Chemical structure of B-FK peptide. C) Competitive binding of 2-(4-hydroxyphenylazo)benzoic acid (HABA) and biotin to avidin (Avi). The amount of B-GGP or B-FK required to saturate a tetrameric Avi was determined using the HABA assay. In the case of B-FK 4 mole equiv saturated the binding sites of Avi, while 5 mole equiv of B-GGP are required to saturate the binding sites of Avi. D) Assembly of neutrophil targeting transporters (GGP)₃-Avi and (FK)₃-Avi.

Figure 4A. Only when the donor–acceptor dye pairs are in close proximity (<10 nm), an energy transfer is observed in the fluorescence spectrum,^[36] which confirms the assembly. Upon excitation at 550 nm in the absorption maximum of Alexa-594 dye (purple star), an emission band was observed at 680 nm, indicating energy transfer from the Avi to B-C3 (Figure 5A, left). No energy transfer was observed for the negative controls (FK)₃-Avi alone or (FK)₃-Avi mixed with nonbiotinylated C3 (Figure 5A, left), thereby corroborating the successful assembly. Upon incubation of the construct at pH 4.5 for 4 h, the FRET is no longer observed (Figure 5A, right), confirming the pH-induced release of C3 in acidic environment. To ensure that the construct can be successfully applied in biological media, the stability of (FK)₃-Avi-C3 was investigated in fetal calf serum (FCS). (FK)₃-Avi-C3 was incubated for up to 24 h in 10% FCS in phosphate buffer saline (PBS) and Western blot analysis was applied to monitor its stability. Notably, no increase in free C3 was observed up to 24 h (Figure 5B), which would have indicated disintegration of the construct. To eliminate false positive due to absorption of C3 by serum proteins, FRET measurements were performed, indicating the presence of molecular and nondegraded (FK)₃-Avi-C3 in 10% FCS (Figure S10, Supporting Information). Taken together, our results show the successful assembly of the (FK)₃-Avi-C3 and (GGP)₃-Avi-C3 constructs with about one C3 per conjugate, thus supporting the postulated formulation.

Furthermore, the release of C3 was induced under acidic conditions in vitro and the constructs remained stable in biological media such as FCS.

2.2. The Supramolecular Complexes (GGP)₃-Avi-C3 and (FK)₃-Avi-C3 are Selectively Internalized into Neutrophil-Like NB-4 Cells and C3 is Released into Their Cytosol

The selective delivery of the Rho-inhibitor C3 into the cytosol of neutrophils by either (GGP)₃-Avi or (FK)₃-Avi was investigated as proof-of-concept for these novel transporter molecules. First, human NB-4 cells, a neutrophil-like cell line, were used to test the ability of (GGP)₃-Avi and (FK)₃-Avi to deliver the C3 Rho-inhibitor into the cytosol of these cells. Therefore, differentiated NB-4 cells were incubated at 37 °C with either (GGP)₃-Avi-C3 or (FK)₃-Avi-C3. For negative controls, the Avi alone and the C3 protein alone were applied. Moreover, cells remained untreated as a further control. The recombinant fusion toxin C2IN-C3lim is a specific Rho inhibitor based on the C3lim enzyme. In combination with the C2IIa transport component of the binary C2 toxin from *C. botulinum* served as positive control.^[37] C2IN-C3lim alone is specifically taken up into monocytic cells, but essentially requires C2IIa for its uptake into the cytosol of other cell types such as epithelial cells. Therefore, in

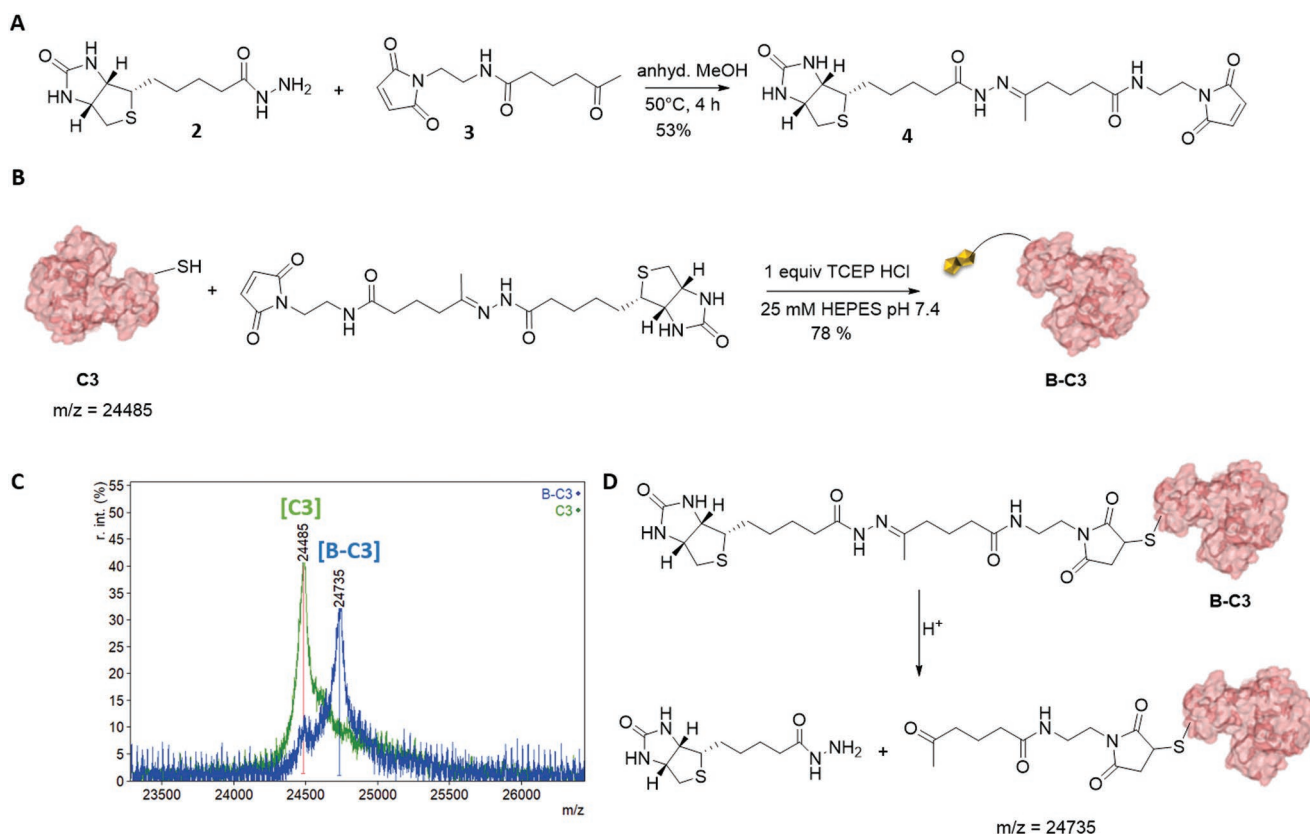


Figure 3. A) Synthesis of compound 4 B) Mono-biotinylation of C3 C) Matrix-assisted laser desorption/ionization (MALDI)-time of flight (ToF) mass spectrometry (MS) spectra of C3 (green) $m/z = 24\ 484$ and biotinylated C3 (B-C3) $m/z = 24\ 735$ using CHCA as matrix. D) Acidic cleavage of B-C3.

combination with C2IIa, the uptake of C2IN-C3lim is not cell-type selective.^[10,37]

In the next step, we determined the characteristic C3-induced changes in cell morphology (Figure 6A) after release of C3 into the cytosol of NB-4 cells. Images of the cells were recorded after different incubation periods and the number of these intoxicated cells was determined based on the morphological changes (Figure 6B). This is a well-established,^[15,17,18,21,35,37,38] highly sensitive and specific endpoint to monitor the uptake of C3 Rho-inhibitor into the host cell cytosol. The changes in cell morphology essentially depend on the C3-catalyzed ADP-ribosylation of Rho in the cytosol.^[15,17,18,21,35,37] As expected, the combination of C2IN-C3lim and C2IIa exhibited the strongest effect while C3 alone and the platform (Avi) alone had almost no effect on cell morphology. Importantly, treatment of NB-4 with (GGP)₃-Avi-C3 as well as (FK)₃-Avi-C3 resulted in a significantly increased number of cells showing the characteristic C3-induced morphology when compared to untreated control cells (Figure 6A,B). This indicates that C3 enzyme activity reached the cytosol of NB-4 cells after their treatment with either (GGP)₃-Avi-C3 or (FK)₃-Avi-C3 ex vivo.

The ability of both transporters to deliver the Rho-inhibitor C3 into the cytosol of NB-4 cells was also confirmed by the biochemical analysis of the ADP-ribosylation status of Rho from these cells and exemplarily shown for (FK)₃-Avi-C3 (Figure 6C). In this assay, the ADP-ribosylation status of Rho was analyzed in cell lysates by sequential ADP-ribosylation with biotin-labeled NAD⁺.^[37,38] A strong signal in the Western blot indicated that

no Rho ADP-ribosylation took place in the intact cells. In contrast, a weak signal in the blot indicated that all/most of the Rho protein have already undergone ADP ribosylation in the intact cells during the incubation with the C3-containing compounds or fusion toxins and therefore is proofed unsuitable as a substrate for the subsequent *in vitro* ADP-ribosylation with biotin NAD⁺. The observation that C3 alone had no comparable effect as (GGP)₃-Avi-C3 or (FK)₃-Avi-C3 regarding the morphology change and the ADP-ribosylation of Rho in the cells indicated that (GGP)₃-Avi or (FK)₃-Avi are essential for the transport of C3 into the cytosol of the neutrophils. Moreover, it excluded the possibility that C3 was separated from the transporters (GGP)₃-Avi or (FK)₃-Avi already in the medium during the incubation with the cells and that some resulting free C3 might have caused the observed effects in the neutrophils independently from the supramolecular transporters.

2.3. Effect of (GGP)₃-Avi-C3 and (FK)₃-Avi-C3 on Primary PMNs Isolated from the Human Blood

After successful demonstration of the transport of the Rho inhibitor C3 into the cytosol of a human neutrophil-like cell line by both supramolecular C3-containing complexes, the effect of (GGP)₃-Avi-C3 and (FK)₃-Avi-C3 on biologically and medically more relevant primary human PMNs was investigated. PMNs were isolated from the blood of healthy human volunteers and incubated at 37 °C with either (GGP)₃-Avi-C3 or

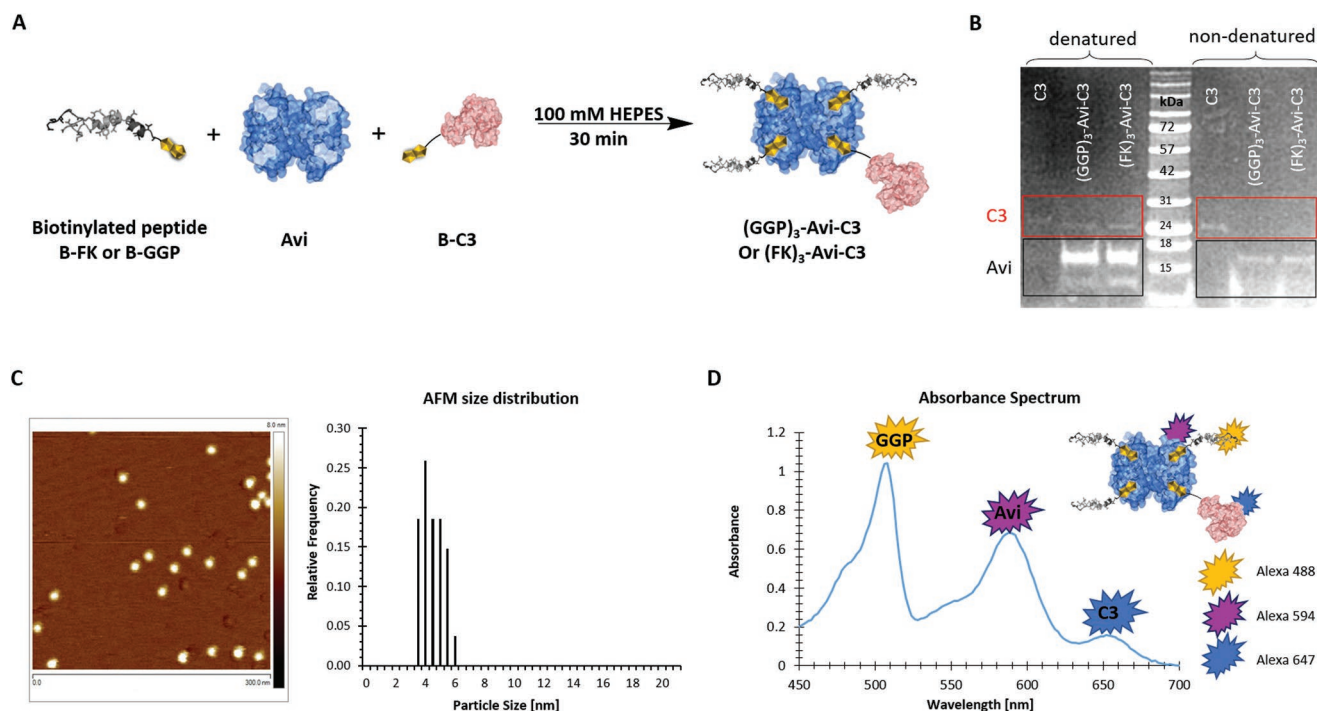


Figure 4. Assembly of the supramolecular complexes $(FK)_3\text{-Avi-C3}$ and $(GGP)_3\text{-Avi-C3}$ and their characterization. A) The controlled assembly of $(GGP)_3\text{-Avi-C3}$ and $(FK)_3\text{-Avi-C3}$ was accomplished through stoichiometric control according to the optimized ratio of 1.25 equiv of B-GGP and 1.0 equiv of B-FK per binding pocket. B) SDS-PAGE characterization of the protein complexes under denaturing and nondenaturing conditions indicate the successful assembly by the disappearance of C3 band under nondenaturing conditions. C) AFM image of $(FK)_3\text{-Avi-C3}$ with height profile analysis of protein particles. D) Absorbance spectrum of $(GGP)_3\text{-Avi-C3}$. Avi was labeled with Alexa-594 dye (purple star), B-C3 was labeled with Alexa-647 dye (blue star) and GGP with Alexa-488 (orange star). The ratio of GGP:Avi:C3 was determined from the absorption envelopes and a ratio of 3.2:1:0.7 was calculated.

$(FK)_3\text{-Avi-C3}$. Images of the cells were taken and the changes in cell morphology were compared with cells left untreated or treated with either Avi alone or C3 alone. The fusion toxin, C2IN-C3lim+ C2IIa, where C2IIa delivers the Rho-inhibitor C2IN-C3lim into the cytosol of all cell types, served as positive control. Like the NB-4 cells, the human PMNs responded with significant changes in cell morphology to the treatment with either $(GGP)_3\text{-Avi-C3}$ or $(FK)_3\text{-Avi-C3}$ and C2IN-C3lim + C2IIa (Figure 7A–C). However, neither Avi nor C3 had a comparable effect (Figure 7A,C). These results clearly indicated that $(GGP)_3\text{-Avi-C3}$ and $(FK)_3\text{-Avi-C3}$ were able to deliver C3 into the cytosol of primary human PMNs. Moreover, $(GGP)_3\text{-Avi}$ as well as $(FK)_3\text{-Avi}$, but not Avi alone, bound to the surface of PMNs at 4 °C as analyzed by flow cytometry, confirming the specific function of the PMN targeting peptides (Figure 7D).

In contrast, neither $(GGP)_3\text{-Avi-C3}$ nor $(FK)_3\text{-Avi-C3}$ showed similar effects on the morphology of human lung epithelial cells A549 (Figure 8A and Figure S11A, Supporting Information) or the recently established human alveolar epithelial cell line hAELVi (Figure 8C and Figure S11B, Supporting Information), a model for the air–blood barrier of the peripheral lung,^[39] implicating that in these cells, the Rho-inhibitor C3 was not delivered into the cytosol by the supramolecular complexes. These findings were confirmed by the biochemical evaluation of the ADP-ribosylation status of Rho of these cells (Figure 8B,D). Our results clearly indicate that C3 enzyme activity was not present in the cytosol of these epithelial cells. On the other hand, treatment of the A549 cells with C2IN-C3lim + C2IIa resulted in the expected C3-induced change

in cell morphology (Figure 8A and Figure S11A, Supporting Information) and the strong ADP-ribosylation of Rho in the cytosol of the living cells by C3 (Figure 8B,D).

3. Conclusion

In conclusion, PMN-targeting supramolecular multiprotein complexes consisting of the specific Rho-inhibitor C3, Avi as molecular glue and three PMN-targeting peptides were prepared by convenient “mix-and-match” assembly using Avi/biotin technology to inhibit Rho-mediated signal transduction in PMNs. $(GGP)_3\text{-Avi-C3}$ or $(FK)_3\text{-Avi-C3}$ were generated, characterized and their biological mode of action was evaluated in vitro and ex vivo. A set of cell-based experiments clearly underlined the efficient and cell type-selective transport of the Rho-inhibitor C3 into the cytosol of primary human PMNs ex vivo and into the cytosol of human neutrophil-like NB-4 cells but not into human lung epithelial cells, which provides strong evidence for cell type-selectivity of $(GGP)_3\text{-Avi}$ and $(FK)_3\text{-Avi}$. We envision that our strategy provides new therapeutic avenue for diseases such as post-traumatic injury of multiple injured patients, which are associated with hyperactivity and reactivity of PMNs.

Based on these seminal proof-of-concept investigations, future studies will focus on the application of the novel supramolecular complexes containing C3 Rho-inhibitor to elucidate whether inhibition of Rho-mediated signal transduction interferes with migration and chemotaxis of human PMNs in trans-well and human “lung-on-a-chip” approaches ex vivo.

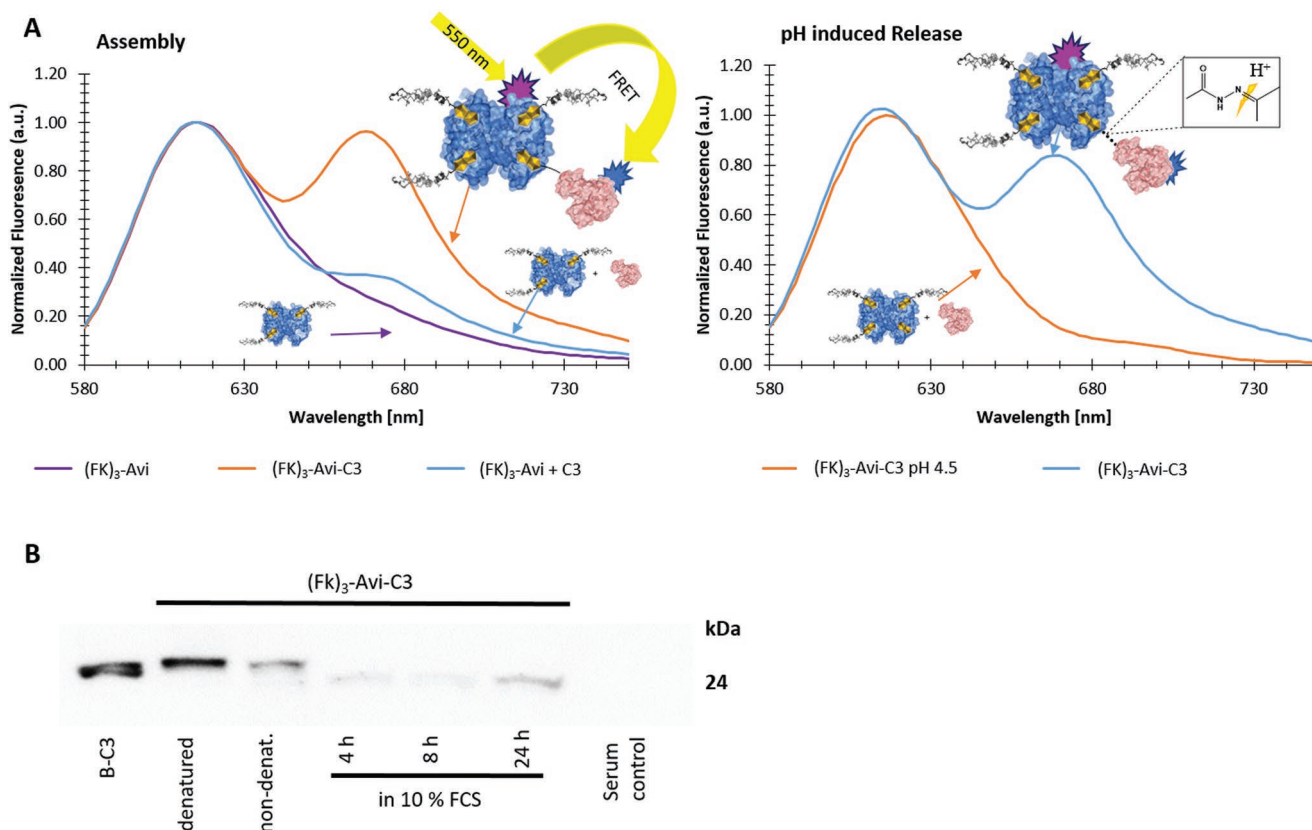


Figure 5. A) Left: Emission spectrum of dual-labeled assembled construct (FK)₃-Avi-C3 (blue), showing FRET and Avi (purple), (FK)₃-Avi + C3, mixed (orange) as control. right: pH induced release, showing no FRET after 4 h incubation time at pH 4.5. B) Stability of (FK)₃-Avi-C3 protein complex in fetal calf serum (FCS). Western blot analysis showed no significant increase up to 24 h. B-C3 and (FK)₃-Avi-C3 in PBS as well as 10% FCS were applied as control.

Moreover, it will be tested by our established animal model whether the local intratracheal application of the novel supra-molecular C3-containing complexes decreases the enhanced invasion of PMNs from the blood into the lungs of mice after blunt thorax trauma. This approach is inspired by earlier proof-of-concept studies which indicate that the intratracheal application of the recombinant Rho-inhibiting C3IN-C3lim fusion toxin significantly reduced the amount of monocytic cells in the lungs of mice after blunt thorax trauma, but had no effect on PMNs because of its cell type-selectivity.^[11] Besides, the stability of the complexes in vivo, e.g., in human blood will also be investigated. Ultimately, we envision the application of supramolecular toxin complexes to downmodulate excessive PMN recruitment and migration across the disturbed alveolar barrier of patients after trauma—a hallmark event in the progression of Acute Lung Injury and Acute Respiratory Distress Syndrome.^[40,41]

4. Experimental Section

General information, methods for AFM, dynamic light scattering (DLS), Zeta-potential, SDS-PAGE and Western blot analysis are provided in the Supporting Information.

Materials: Unless otherwise stated, all chemicals were obtained from commercial sources (Merck, Sigma Aldrich, Fluka and Thermo Scientific, Fisher Scientific) and used without further purification. All organic

solvents (acetonitrile (CH₃CN), chloroform (CHCl₃), dichloromethane (DCM), dimethylformamide (DMF), dimethyl sulfoxide (DMSO), methanol (MeOH)) were obtained from Fisher Scientific and used without further purification (HPLC or analytical grades). The peptides Ac-GGPNLTGRWGPPVESALAK-NH₂ (GGP) and cFLFLFK-Biotin (B-FK) were purchased from PhtdPeptides Co., Ltd. (Zhengzhou City, China) with 95% purity. Water used for the reactions was obtained from the Merck Millipore purification system.

Cell culture media (Dulbecco's modified Eagle's medium (DMEM), Roswell Park Memorial Institute (RPMI) 1640 Medium) and fetal calf serum were from Gibco Life Technologies (Karlsruhe, Germany), cell culture materials from TPP (Trasadingen, Switzerland) and Sarstedt (Nümbrecht, Germany). Monovettes were from Sarstedt (Nümbrecht, Germany) and Biocoll Separating Solution from Biochrom GmbH (Berlin, Germany). Penicillin–streptomycin and Page Ruler prestained protein ladder were purchased from Thermo Fisher Scientific (Ulm, Germany). Page Ruler unstained protein ladder was purchased from GE Healthcare Life Sciences (Uppsala, Sweden). Complete protease inhibitor and streptavidin–peroxidase were from Roche (Mannheim, Germany) and biotinylated NAD⁺ from R&D Systems GmbH (Wiesbaden-Nordenstadt, Germany). The antibody against GAPDH and the peroxidase-coupled antimouse binding protein were from Santa Cruz Biotechnology (Heidelberg, Germany). Thrombin was purchased from Sigma-Aldrich Chemie GmbH (Steinheim, Germany), the nitrocellulose blotting membrane from GE Healthcare Life Sciences (Uppsala, Sweden), and the enhanced chemiluminescence (ECL) system from Millipore (Schwalbach, Germany). All-trans-retinoic acid (ATRA) and *N,N'*-hexamethylene bis(acetamide) (HMBA) were from Sigma-Aldrich (Steinheim, Germany). G-CSF was purchased from Sino Biological Inc. (Wayne, PA, USA). The expression, purification and biochemical

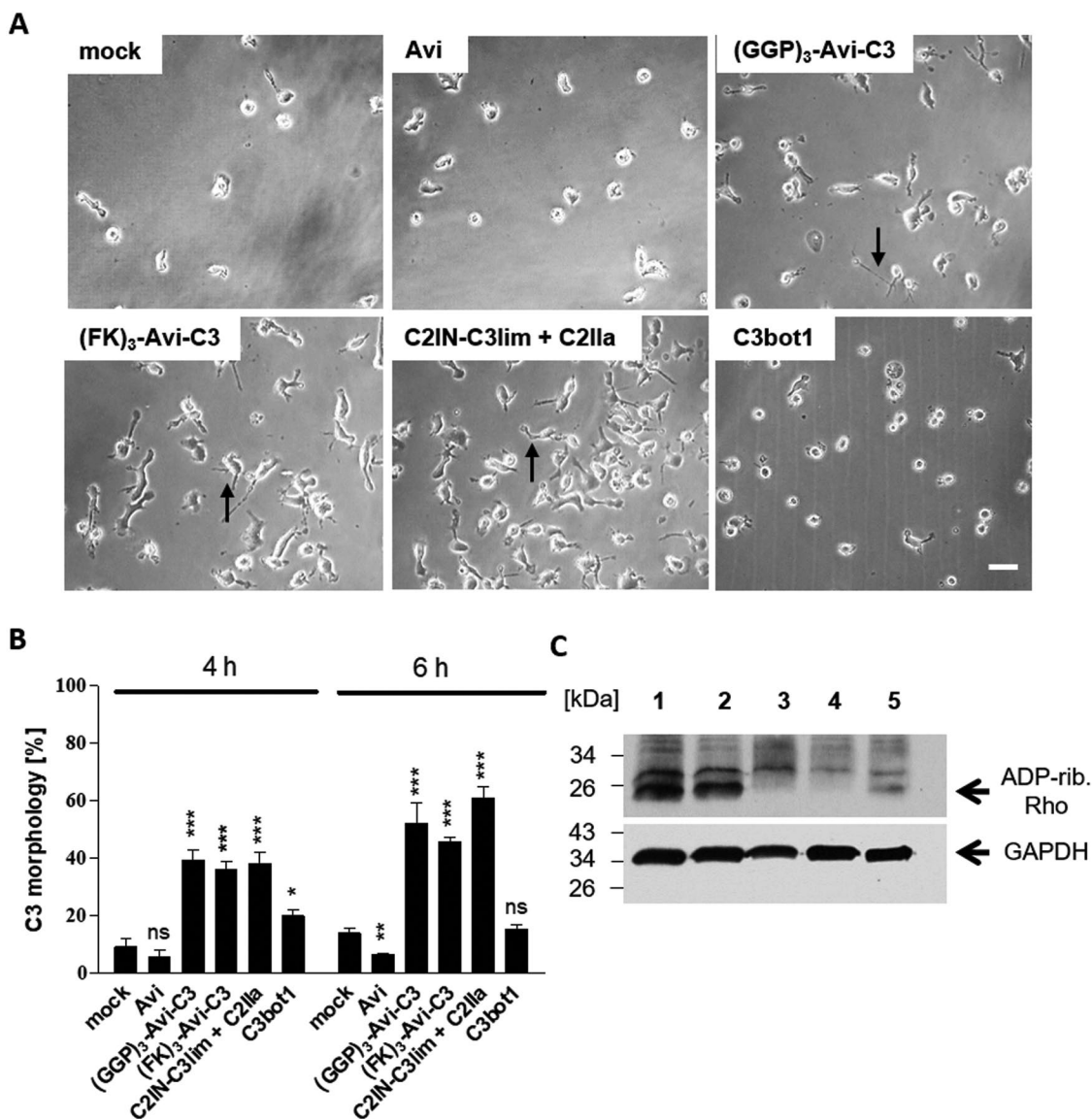


Figure 6. Effect of (GGP)₃-Avi-C3 and (FK)₃-Avi-C3 on human neutrophil-like NB-4 cells. A) Differentiated NB-4 cells were incubated with 320×10^{-9} M Avi, 320 nM (GGP)₃-Avi-C3, 320×10^{-9} M (FK)₃-Avi-C3, $1 \mu\text{g mL}^{-1}$ C2IN-C3lim + $2 \mu\text{g mL}^{-1}$ C2IIa, 320×10^{-9} M C3bot1 or left untreated for control (mock). The cells were incubated at 37°C and cell morphology was observed by phase contrast microscopy and documented over 6 h. The arrows indicate cells showing characteristic changes in cell morphology induced by the C3 Rho-inhibitor. The scale bar represents $50 \mu\text{m}$. B) Quantitative analysis of NB-4 cells showing the C3-induced morphology from pictures after 4 and 6 h. Values are given as mean \pm SEM ($n = 6$). Significance was tested using Student's *t*-test (ns, not significant, $*p < 0.05$, $**p < 0.01$, $***p < 0.001$). C) Analysis of the ADP-ribosylation status of these cells. The cells were treated as described in (A) and subsequently lysed. Equal amount of lysate protein of each sample was subjected to *in vitro* ADP-ribosylation with C3 enzyme and biotin-NAD⁺. The biotinylated, i.e., ADP-ribosylation of Rho was detected by Western blotting (upper panel). Note: A strong signal in the blot indicates that no ADP-ribosylation of Rho took place in the living cells, demonstrating that the C3 Rho-inhibitor was not present in their cytosol. A weak signal indicates that most ADP-ribosylation of the Rho protein took already place in the cytosol of the living cells by C3 Rho-inhibitor during the incubation period, indicating that active C3 enzyme reached the cytosol of these cells. Lower panel: GAPDH-staining to demonstrate comparable protein loading and blotting. 1) mock, 2) Avi, 3) (FK)₃-Avi-C3, 4) C2IN-C3lim + C2IIa, 5) C3.

characterization of the recombinant proteins C2IIa, C2IN-C3lim, and cysteine mutant of C3 was performed as described earlier.^[16,20,21]

Synthesis of (E)-N-(2-(2,5-dioxo-2,5-dihydro-1H-pyrrol-1-yl)ethyl)-5-(2-(5-((3aS,4S,6aR)-2-oxohexahydro-1H-thieno[3,4-d]imidazol-4-yl)pentanoyl)hydrazineylidene)hexanamide 4: N-(2-(2,5-dioxo-2,5-dihydro-1H-pyrrol-1-yl)ethyl)-5-oxohexamide (63 mg, 0.25 mmol, 1 equiv) and 5-((3aS,4S,6aR)-2-oxohexahydro-1H-thieno[3,4-d]imidazol-4-yl)pentanohydrazide (78 mg, 0.3 mmol, 1.2 equiv) were dissolved in 10 mL anhydrous MeOH under argon atmosphere. The resulting reaction

mixture was heated to 50°C and was continuously stirred for 4 h. The solvent was removed under high vacuum, and the residue was purified by column chromatography using eluting solvents 10% MeOH in DCM to afford 63 mg (0.12 mmol, 53%) of the final product; ¹H-NMR (300 MHz, MeOD δ) 6.83 (s, 2H) 4.51 (m, 1H) 4.33 (m, 1H), 3.63 (m, 2H), 3.36 (m, 2H), 3.22 (m, 1H), 2.94 (d, 1H, $J = 12.7$ Hz), 2.71 (d, 1H, $J = 12.7$ Hz), 2.11–2.44 (m, 6H), 1.98 (1H), 3.36 (m, 2H), 3.63 (m, 2H), 4.33 (m, 1H), 4.51 (m, 1H), 6.83 (s, 2H). ¹³C-NMR (100 MHz, MeOD, δ) 176.20, 172.56, 165.93, 162.15, 135.45, 127.34, 63.41, 61.63, 56.96,

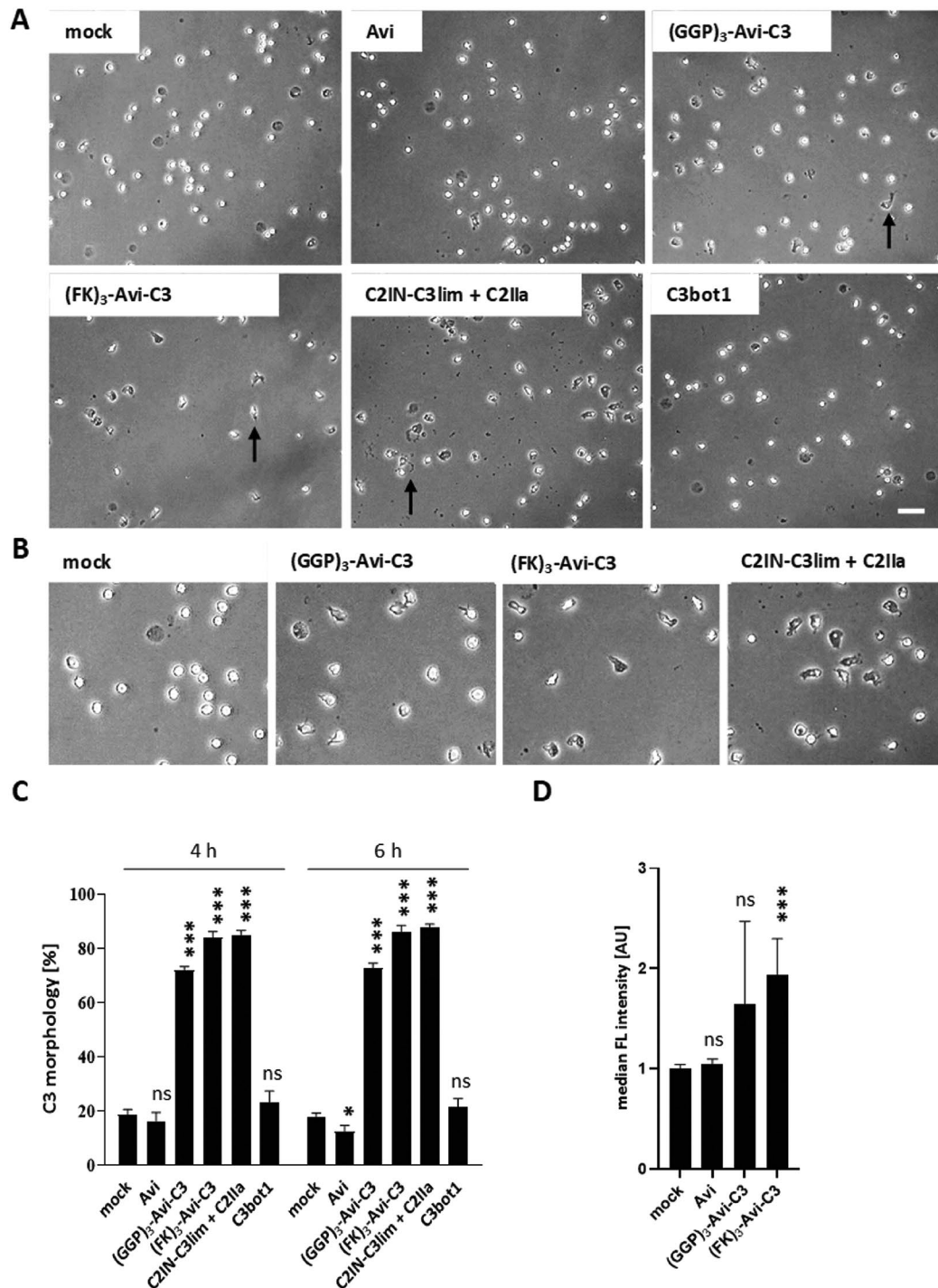


Figure 7. Effect of (GGP)₃-Avi-C3 and (FK)₃-Avi-C3 on primary human PMNs ex vivo. A) PMNs were isolated from blood of healthy donors and then treated ex vivo with 320×10^{-9} M Avi, 320×10^{-9} M (GGP)₃-Avi-C3, 320×10^{-9} M (FK)₃-Avi-C3, $1 \mu\text{g mL}^{-1}$ C2IN-C3lim + $2 \mu\text{g mL}^{-1}$ C2IIa, 320×10^{-9} M C3 or left untreated for control (mock). Cells were incubated at 37°C and cell morphology was observed over a period of 6 h. Arrows indicate cells showing the characteristic changes in cell morphology induced by C3 Rho-inhibitor. The scale bar represents $50 \mu\text{m}$. B) Cells of the same experiment with typical C3-induced morphology were enlarged for better visualization. C) Quantitative analysis of cells showing the C3-induced morphology from pictures after 4 and 6 h. Values are given as mean \pm SEM ($n = 9$). Significance was tested using Student's *t*-test (ns, not significant, $*p < 0.05$, $***p < 0.001$). D) Analysis of the binding of (GGP)₃-Avi-C3 and (FK)₃-Avi-C3 to PMNs by flow cytometry. PMNs (200 000 cells in $200 \mu\text{L}$ complete medium) were incubated for 10 min at 4°C with either Avi, (GGP)₃-Avi-C3, or (FK)₃-Avi-C3 (all labeled with bodipy-fl (BDP)) or left untreated for control (mock). Subsequently, the cells were washed and analyzed by flow cytometry for the cell-bound BDP-proteins. The median fluorescence (FL) intensity of the respective histogram peaks was calculated, normalized to untreated control (mock) and is shown as arbitrary units (AU). Values are given as mean \pm SEM ($n = 5$). Significance was tested using Student's *t*-test (ns, not significant, $***p < 0.001$).

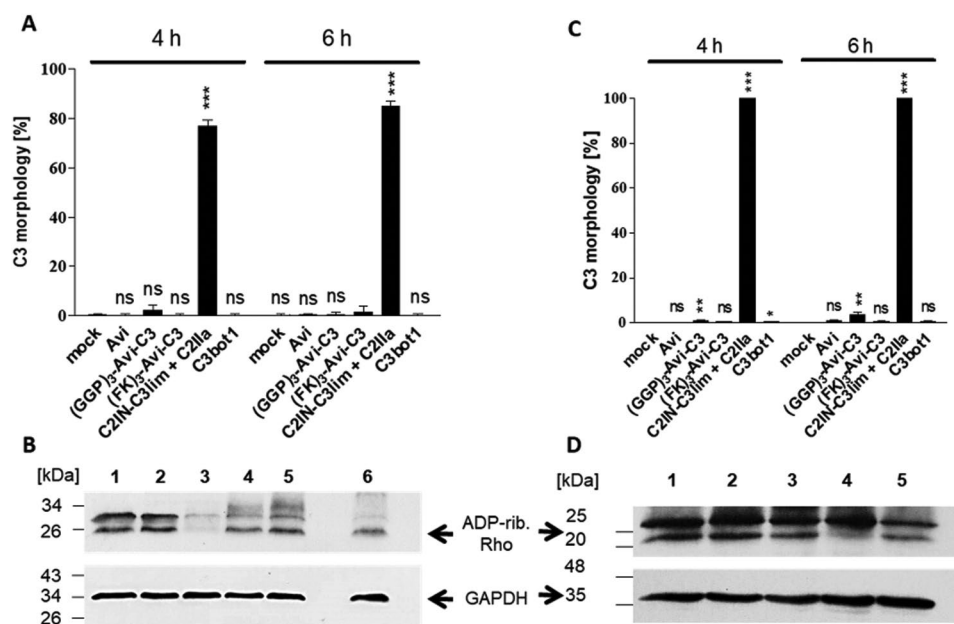


Figure 8. Effect of (GGP)₃-Avi-C3 and (FK)₃-Avi-C3 on human A549 lung cancer epithelial cells and on the human alveolar epithelial cell line hAELVi. A) A549 cells were treated with 320 × 10⁻⁹ M Avi, 320 × 10⁻⁹ M (GGP)₃-Avi-C3, 320 × 10⁻⁹ M (FK)₃-Avi-C3, 1 μg mL⁻¹ C21N-C3lim + 2 μg mL⁻¹ C21Ia, 320 × 10⁻⁹ M C3 or left untreated for control (mock). Cells were incubated at 37 °C and cell morphology was analyzed after a period of 4 and 6 h. Values are given as mean ± SD (n = 3). Significance was tested using Student's *t*-test (ns, not significant, ****p* < 0.001). B) Analysis of the ADP-ribosylation status of these cells. The cells were treated as described in (A) and then lysed. Equal amount of lysate protein of each sample was subjected to in vitro ADP-ribosylation with C3 enzyme and biotin-NAD⁺. The biotinylated, i.e., ADP-ribosylation of Rho was detected by Western blotting (upper panel). A strong signal in the blot indicates that no ADP ribosylation of Rho took place in the living cells, demonstrating that no C3 Rho-inhibitor was present in their cytosol. A weak signal indicates that most ADP-ribosylation of the Rho took already place in the cytosol, of the living cells during the incubation period. Lower panel: GAPDH-staining to demonstrate comparable protein loading and blotting. 1) mock, 2) Avi, 3) (FK)₃-Avi-C3, 4) C21N-C3lim + C21Ia, 5) C3, 6) (GGP)₃-Avi-C3. C) hAELVi cells were treated with 320 × 10⁻⁹ M Avi, 320 × 10⁻⁹ M (GGP)₃-Avi-C3, 320 × 10⁻⁹ M (FK)₃-Avi-C3, 3 μg mL⁻¹ C21N-C3lim + 6 μg mL⁻¹ C21Ia, 320 × 10⁻⁹ M C3 or left untreated for control (mock). Cells were incubated at 37 °C and cell morphology was analyzed after a period of 4 and 6 h. Values are given as mean ± SEM (n = 9). Significance was tested using Student's *t*-test (ns, not significant, **p* < 0.05, ***p* < 0.01, ****p* < 0.001). D) Analysis of the ADP-ribosylation status of these cells. The cells were treated as described in (C) and then lysed. Equal amount of lysate protein of each sample was subjected to in vitro ADP-ribosylation with C3 enzyme and biotin-NAD⁺. The biotinylated, i.e., ADP-ribosylation of Rho was detected as described in (B) 1) mock, 2) Avi, 3) (FK)₃-Avi-C3, 4) C21N-C3lim + C21Ia, 5) C3.

41.03, 38.89, 38.41, 38.26, 35.68, 34.59, 29.80, 29.53, 26.62, 23.53, 16.54. Liquid chromatography–mass spectrometry (LC–MS): *T_R*: 3.51 min, *m/z*: 493 [M+H]⁺, 515 [M+Na]⁺, 253 [2+Na]⁺ (calcd. mass: 492.22, formula: C₂₂H₃₂N₆O₅S).

Biotinylation of Ac-GGPNLTGRWGPPVESALAK-NH₂ (B-GGP): A 2 mg mL⁻¹ solution of GGP-peptide (5 mg, 2.5 μmol) in DMF and a 1 mg mL⁻¹ solution of biotin-(PEO)₃-maleimide in phosphate buffer (50 × 10⁻³ M, pH 7.4) were mixed and incubated overnight at RT under shaking. The respective solution was lyophilized and washed with DCM to remove unreacted biotin reagent. The crude product was further purified by HPLC using a XDB-C18 column with the mobile phase starting from 100% solvent A (0.1% TFA in water) and 0% solvent B (0.1% TFA in acetonitrile) (0–5 min) with a flow rate of 4 mL min⁻¹, raising to 5% solvent B in 5 min, 15% solvent B in 10 min, and then reaching 100% solvent B after 29 min. It remained in this state for 1 min. Solvent B concentration was then finally lowered to 5% over five minutes. Absorbance was monitored at 280 and 254 nm. The retention time for GGP-B was 17.5 min, and 2.75 mg (1.02 μmol, 40%) of the product was obtained after lyophilization; LC–MS: *T_R*: 4.51, *m/z*: 898 [M+3H]³⁺. MALDI-ToF-MS (CHCA): *m/z*: 2691 [M+H]⁺, 2713 [M+Na]⁺ (calcd. mass: 2689 formula: C₁₂₀H₁₉₂N₃₂O₃₄S₂).

Biotinylation of C3 (B-C3): The recombinant cysteine mutant of C3 was expressed and purified in *Escherichia coli* BL21 as described in the literature.^[35]

60 μL of 4-(2-hydroxyethyl)-1-piperazine–ethanesulfonic acid (HEPES) buffer (100 × 10⁻³ M, pH 7.4) and tris(2-carboxyethyl)phosphine (TCEP) HCl were sequentially added to the C3 solution (200 μg,

8 nmol, 1 equiv) and were incubated for 30 min at RT under shaking. Subsequently, 30 μL of compound **3** (5 mg mL⁻¹ in DMF, 30 equiv) were added to the reaction mixture and the resulting mixture was shaken for 3 h at 4 °C. Thereafter, rigorous ultrafiltration with 3 × 500 μL buffer (molecular weight cut off (MWCO) = 10 kDa, 25 × 10⁻³ M HEPES buffer, pH 7.4) was used to remove excess of compound **3** to yield 208 μL B-C3 (0.7 mg mL⁻¹, 73% yield). The concentration of B-C3 was determined using a bicinchoninic acid (BCA) assay (A562 nm) with BSA as reference. Successful biotinylation was confirmed by MALDI-ToF-MS (Figure 3C) and degree of labeling was quantified by Quant*Tag Biotin Kit at A535 nm.

Assembly of Transport Proteins (GGP)₃-Avi and (FK)₃-Avi: (GGP)₃-Avi was assembled by dissolving 2 mg (31.7 nmol, 1 equiv) of Avi-BDP in 1 mL phosphate buffer (50 × 10⁻³ M, pH 7.4) and subsequent adding 383 μL GGP-B (383 μg in MilliQ water, 143 nmol, 4.5 equiv). The mixture was incubated for 1 h at RT under shaking and purified by rigorous ultracentrifugation (MWCO = 20 kDa, using 3 × 500 μL 50 × 10⁻³ M phosphate buffer pH 7.4). (FK)₃-Avi was assembled by dissolving 1 mg (15.9 nmol, 1 equiv) Avi-BDP in 1 mL phosphate buffer (50 × 10⁻³ M, pH 7.4) and 5.57 μL FK-B (56 μg in DMSO, 47.7 nmol, 3 equiv) were subsequently added. The mixture was incubated for 1 h at RT under shaking and purified by ultracentrifugation (MWCO = 20 kDa, using 3 × 800 μL 50 × 10⁻³ M phosphate buffer pH 7.4).

Assembly of (GGP)₃-Avi-C3 and (FK)₃-Avi-C3: (FK)₃-Avi-C3 was assembled by using 66 μL Avi-BDP (2 mg mL⁻¹ in HEPES buffer 25 × 10⁻³ M, pH 7.4) dissolved in 100 μL of HEPES buffer (50 × 10⁻³ M, pH 7.4). Then, 62 μL (0.8 mg mL⁻¹ in 25 × 10⁻³ M HEPES buffer pH 7.4,

50 μg , 2.0 nmol, 1 equiv) of B-C3 and 0.7 μL of B-FK (1 mg mL^{-1} in DMSO, 6.0 nmol, 3 equiv) were added.

(GGP)₃-Avi-C3 was assembled by using 66 μL (2 mg mL^{-1} in HEPES buffer 25×10^{-3} M, pH 7.4) of Avi-BDP dissolved in 100 μL of HEPES buffer (50×10^{-3} M, pH 7.4) and adding 62 μL (0.8 mg mL^{-1} in 25×10^{-3} M HEPES buffer pH 7.4, 50 μg , 2.0 nmol, 1 equiv) of B-C3 and 24 μL of B-GGP (1 mg mL^{-1} in MilliQ water, 9.0 nmol, 4.5 equiv).

Analysis of the ADP-Ribosylation Status of Rho in Cells: To analyze the ADP-ribosylation of Rho in the cytosol of cells, in vitro ADP-ribosylation with biotin-labeled NAD⁺ as cosubstrate and C3 enzyme was performed as described earlier.^[11,17,37] In brief, cells were incubated at 37 °C with the respective transporters and toxins or left untreated for control as described in the previous section. Then, the cells were lysed and equal amount of lysate protein was incubated with 10×10^{-3} M biotin-labeled NAD⁺ and 300 ng C3 for 30 min at 37 °C. The enzyme reaction was terminated by adding SDS sample buffer and boiling the samples at 95 °C for 10 min. The biotinylated, i.e., ADP-ribosylation of Rho was detected by Western blotting with streptavidin-peroxidase using the ECL system. To confirm comparable amount of blotted protein, GAPDH was detected in addition.

Flow Cytometry: PMNs were isolated as described before. For flow cytometry analysis 2×10^5 cells in 100 μL RPMI + 1% FCS were incubated with Avi (320×10^{-9} M), (GGP)₃-Avi-C3 (320×10^{-9} M), or (FK)₃-Avi-C3 (320×10^{-9} M) for 10 min on ice to prevent an endocytic uptake. Cells were washed with ice-cold PBS, resuspended in 200 μL complete medium and analyzed by flow cytometry using BD FACSCelesta flow cytometer and the BD FACSDiva software. BDP was excited with a blue laser (488 nm), emitted fluorescence was detected with a 530 nm (530/30) bandpass filter. Analysis and creation of fluorescence histograms from gated cell populations was performed using Flowing Software v2.5.1 (Perttu Terho, Turku Centre for Biotechnology, Finland).

Statistical Analysis: Preprocessing of data was performed as described in each experimental section. The results were presented as mean \pm SD or mean \pm SEM as described in each figure description. Sample sizes are given in figure legends or as described in this section. Analyses comparing means of different treatment groups were performed using Student's test (GraphPad Prism 5; GraphPad Software, Inc.) and *p* values less than 0.05 were considered significant.

Supporting Information

Supporting Information is available from the Wiley Online Library or from the author.

Acknowledgements

A.J.H. and T.O. contributed equally to this work. The authors are grateful to the Max Planck Society and the Deutsche Forschungsgemeinschaft (DFG, German Research Foundation) project number 251293561-SFB 1149, Projects A04, A05; project number 316249678-SFB 1279, Projects C01, C02. T.W. acknowledges the support of the ERC Synergy Grant under grant agreement no. 319130 (BioQ).

Conflict of Interest

The authors declare no conflict of interest.

Keywords

C3 Rho inhibitor, polymorphonuclear leukocytes (PMNs), supramolecular toxin complex, targeted protein delivery

Received: May 24, 2019

Revised: July 4, 2019

Published online: July 18, 2019

- [1] A. Kovtun, D. A. C. Messerer, K. Scharffetter-Kochanek, M. Huber-Lang, A. Ignatius, *J. Immunol. Res.* **2018**, 2018, 1.
- [2] M. W. Knoferl, U. C. Liener, D. H. Seitz, M. Perl, U. B. Bruckner, L. Kinzl, F. Gebhard, *Shock* **2003**, 19, 519.
- [3] K. Raghavendran, B. A. Davidson, J. A. Woytash, J. D. Helinski, C. J. Marschke, P. A. Manderscheid, R. H. Notter, P. R. Knight, *Shock* **2005**, 24, 132.
- [4] D. H. Seitz, U. Niesler, A. Palmer, M. Sulger, S. T. Braumuller, M. Perl, F. Gebhard, M. W. Knoferl, *Crit. Care Med.* **2010**, 38, 1852.
- [5] U. Niesler, A. Palmer, J. S. Froba, S. T. Braumuller, S. Zhou, F. Gebhard, M. W. Knoferl, D. H. Seitz, *J. Trauma Acute Care Surgery* **2014**, 76, 386.
- [6] C. D. Nobes, A. Hall, in *Bacterial Toxins: Tools in Cell Biology and Pharmacology* (Ed: K. Aktories), Wiley-Blackwell, Hoboken, NJ **1993**, Ch. 6.
- [7] C. Laudanna, J. J. Campbell, E. C. Butcher, *Science* **1996**, 271, 981.
- [8] L. Liu, B. R. Schwartz, N. Lin, R. K. Winn, J. M. Harlan, *J. Immunol.* **2002**, 169, 2330.
- [9] A. P. Wheeler, A. J. Ridley, *Exp. Cell Res.* **2007**, 313, 3505.
- [10] H. Barth, S. Fischer, A. Moglich, C. Fortsch, *Front. Immunol.* **2015**, 6, 6.
- [11] T. Martin, A. Moglich, I. Felix, C. Fortsch, A. Rittlinger, A. Palmer, S. Denk, J. Schneider, L. Notbohm, M. Vogel, H. Geiger, S. Paschke, M. Huber-Lang, H. Barth, *Arch. Toxicol.* **2018**, 92, 323.
- [12] R. T. Jennings, M. Strengert, P. Hayes, J. El-Benna, C. Brakebusch, M. Kubica, U. G. Knaus, *Blood* **2014**, 123, 3635.
- [13] R. A. Worthylake, S. Lemoine, J. M. Watson, K. BurrIDGE, *J. Cell Biol.* **2001**, 154, 147.
- [14] K. Aktories, J. Frevert, *Biochem. J.* **1987**, 247, 363.
- [15] P. Chardin, P. Boquet, P. Madaule, M. R. Popoff, E. J. Rubin, D. M. Gill, *EMBO J.* **1989**, 8, 1087.
- [16] M. Vogelsang, A. Pautsch, K. Aktories, *Naunyn-Schmiedeberg's Arch. Pharmacol.* **2007**, 374, 347.
- [17] J. Fahrer, J. Kuban, K. Heine, G. Rupps, E. Kaiser, E. Felder, R. Benz, H. Barth, *Cell. Microbiol.* **2010**, 12, 233.
- [18] A. Tautzenberger, C. Förtsch, C. Zwerger, L. Dmochewitz, L. Kreja, A. Ignatius, H. Barth, *PLoS One* **2013**, 8, e85695.
- [19] J. Rotsch, A. Rohrbeck, M. May, T. Kolbe, S. Hagemann, I. Schelle, I. Just, H. Genth, S. C. Huelsenbeck, *Naunyn-Schmiedeberg's Arch. Pharmacol.* **2012**, 385, 883.
- [20] A. Rohrbeck, L. von Elsner, S. Hagemann, I. Just, *Toxins* **2015**, 7, 380.
- [21] J. Gacanin, A. Kovtun, S. Fischer, V. Schwager, J. Quambusch, S. L. Kuan, W. N. Liu, F. Boldt, C. Li, Z. Q. Yang, D. S. Liu, Y. Z. Wu, T. Weil, H. Barth, A. Ignatius, *Adv. Healthcare Mater.* **2017**, 6, 1700392.
- [22] D. L. Jaye, F. S. Nolte, L. Mazzucchelli, C. Geigerman, A. Akyildiz, C. A. Parkos, *Am. J. Pathol.* **2003**, 162, 1419.
- [23] D. L. Jaye, H. A. Edens, L. Mazzucchelli, C. A. Parkos, *J. Immunol.* **2001**, 166, 7250.
- [24] L. Mazzucchelli, J. B. Burritt, A. J. Jesaitis, A. Nusrat, T. W. Liang, A. T. Gewirtz, F. J. Schnell, C. A. Parkos, *Blood* **1999**, 93, 1738.
- [25] E. Karathanasis, C. M. Geigerman, C. A. Parkos, L. Chan, R. V. Bellamkonda, D. L. Jaye, *Ann. Biomed. Eng.* **2009**, 37, 1984.
- [26] L. W. Locke, M. D. Chordia, Y. Zhang, B. Kundu, D. Kennedy, J. Landseadel, L. Xiao, K. D. Fairchild, S. S. Berr, J. Linden, D. Pan, *J. Nucl. Med.* **2009**, 50, 790.
- [27] J. Pellico, A. V. Lechuga-Vieco, E. Almarza, A. Hidalgo, C. Mesa-Nunez, I. Fernandez-Barahona, J. A. Quintana, J. Bueren, J. A. Enriquez, J. Ruiz-Cabello, F. Herranz, *Sci. Rep.* **2017**, 7, 13242.
- [28] A. S. Wayne, D. J. FitzGerald, R. J. Kreitman, I. Pastan, *Blood* **2014**, 123, 2470.
- [29] T. Kohl, C. Schmidt, S. Wiemann, A. Poustka, U. Korf, *Proteome Sci.* **2008**, 6, 4.
- [30] S. L. Kuan, D. Y. W. Ng, Y. Z. Wu, C. Fortsch, H. Barth, M. Doroshenko, K. Koynov, C. Meier, T. Weil, *J. Am. Chem. Soc.* **2013**, 135, 17254.

- [31] S. L. Kuan, F. R. G. Bergamini, T. Weil, *Chem. Soc. Rev.* **2018**, *47*, 9069.
- [32] Y. Z. Wu, D. Y. W. Ng, S. L. Kuan, T. Weil, *Biomater. Sci.* **2015**, *3*, 214.
- [33] S. L. Kuan, C. Fortsch, D. Y. W. Ng, S. Fischer, Y. Tokura, W. N. Liu, Y. Z. Wu, K. Koynov, H. Barth, T. Weil, *Macromol. Biosci.* **2016**, *16*, 803.
- [34] P. Moscariello, D. Y. W. Ng, M. Jansen, T. Weil, H. J. Luhmann, J. Hedrich, *Adv. Sci.* **2018**, *5*, 1700897.
- [35] S. L. Kuan, S. Fischer, S. Hafner, T. Wang, T. Syrovets, W. Liu, Y. Tokura, D. Y. W. Ng, A. Riegger, C. Förtsch, D. Jäger, T. F. E. Barth, T. Simmet, H. Barth, T. Weil, *Adv. Sci.* **2018**, *5*, 1701036.
- [36] A. K. Kenworthy, *Methods* **2001**, *24*, 289.
- [37] H. Barth, F. Hofmann, C. Olenik, I. Just, K. Aktories, *Infect. Immun.* **1998**, *66*, 1364.
- [38] I. Just, C. Mohr, G. Schallehn, L. Menard, J. R. Didsbury, J. Vandekerckhove, J. van Damme, K. Aktories, *J. Biol. Chem.* **1992**, *267*, 10274.
- [39] A. Kuehn, S. Kletting, C. de Souza Carvalho-Wodarz, U. Repnik, G. Griffiths, U. Fischer, E. Meese, H. Huwer, D. Wirth, T. May, N. Schneider-Daum, C. M. Lehr, *Altex* **2016**, *33*, 251.
- [40] C. Sharp, A. B. Millar, A. R. Medford, *Respiration* **2015**, *89*, 420.
- [41] M. A. Matthay, R. L. Zemans, *Annu. Rev. Pathol.: Mech. Dis.* **2011**, *6*, 147.